Optimization of Partial Differential Equations for Minimizing the Roughness of Laser Cutting Surfaces

Georg Vossen, Jens Schüttler and Markus Nießen

Lehr- und Forschungsgebiet Nichtlineare Dynamik der Laserfertigungsverfahren, RWTH Aachen, Steinbachstr. 15, 52074 Aachen
georg.vossen@nld.rwth-aachen.de, jens.schuettler@nld.rwth-aachen.de and markus.niessen@nld.rwth-aachen.de

Summary. This work introduces a mathematical model for laser cutting which involves two coupled nonlinear partial differential equations. The model will be investigated by linear stability analysis to study the occurence of ripple formations at a cutting surface. We define a measurement for the roughness of the cutting surface and give a method for minimizing the roughness with respect to process parameters. A numerical solution of this nonlinear optimization problem will be presented and compared with the results of the linear stability analysis.

1 Introduction

Laser cutting is a thermal separation process widely used in shaping and contour cutting applications. There are, however, gaps in understanding the dynamics of the process, especially issues related to cut quality. One essential problem in laser cutting is the occurence of ripple structures at the cutting surface, cf. Figure 1. Such structures can be induced by fluctuations in the

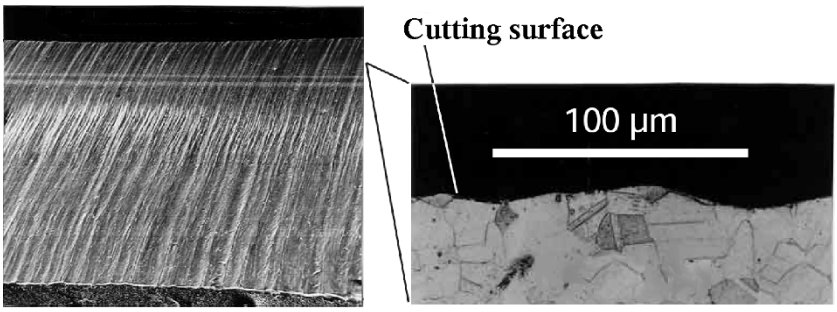

Fig. 1. Image of a cutting surface with ripple structures

M. Diehl et al. (eds.), *Recent Advances in Optimization and its Applications in Engineering*, DOI 10.1007/978-3-642-12598-0_46,

melt flow during the process. Typical tasks in laser cutting applications involve finding process parameters like laser power or cutting speed such that ripple structures at the cutting front are minimal.

Research work has been done in the fields of modeling, model analysis and numerical simulation of laser cutting. One of the major challenges is the treatment of the arising melt and its free boundaries in the process. An overview on state-of-the-art and new developments in the field of modeling on the basis of asymptotic expansions, integral (or variational) methods and spectral methods is presented in [9]. Numerical simulation involving Level Set methods and adaptive sparse grids has been applied in [7]. Nonlinear stability analysis of melt flows has been carried out in [12]. The special problem of ripple formations has been investigated in [10, 3]. An optimization on the basis of the model in the latter reference has been applied in [11].

2 A model for the dynamical behavior of the melt surfaces

We introduce a model in scaled and dimensionless coordinates for the surfaces of the melt arising in a laser cutting process. Figure 2 shows the melt bounded

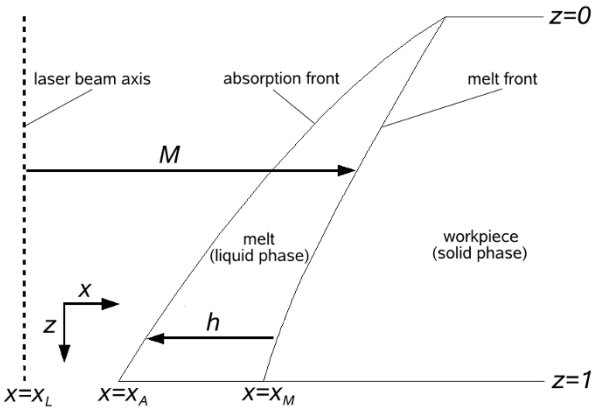

Fig. 2. Schematic 2D view of a laser cutting process

by three free boundaries: the melt front and the absorption front (intersecting at $z = 0$) and the lower boundary along $z = 1$. The position of the laser beam axis (dashed) is $x = x_L := t$ and the laser with beam radius m_0 propagates vertically in z–direction. The melt front with position $x = x_M := x_L + M$ where $M = M(z, t)$ is the distance from the laser beam axis is given by the

phase boundary where molten material from the solid phase enters the liquid phase. The cutting gas expelling the melt downwards and the laser beam hit the melt at the absorption front with position $x = x_A := x_M - h$ where $h = h(z,t)$ is the melt film thickness. It intersects the melt front at $(x,z) = (m_0, 0)$. The lower boundary of the melt is given as the connecting arc between the lower end points of the melt and the absorption front along $z = 1$.

A model for the dynamical behavior of the melt and the absorption front and their interactions is given by the initial/boundary value problem

$$\frac{\partial h}{\partial t} + 2h\frac{\partial h}{\partial z} = v_p, \quad \frac{\partial M}{\partial t} = v_p - 1, \quad v_p = Q_A - Q_s, \quad Q_s = \frac{c_p \Delta T}{H_m} \tag{1}$$

$$Q_A = \nu\mu\mathcal{A}(\mu), \quad \nu = \frac{P_L}{\pi w_0^2 \rho H_m v_0}, \quad \mathcal{A}(\mu) = \frac{4\mu\iota}{2\mu^2 + 2\mu\iota + \iota^2} \tag{2}$$

$$\mu = \alpha\left(\frac{\partial h}{\partial z} - \frac{\partial M}{\partial z}\right), \quad \alpha = \frac{d_m}{d}, \quad d_m = \sqrt{\frac{2\eta_l v_0 d}{\tau_g}} \tag{3}$$

$$h(0,t) = 0, \;\; M(0,t) = m_0 = w_0/d_m, \;\; h(z,0) = h_i(z), \;\; M(z,0) = M_i(z) \tag{4}$$

for z, $t \geq 0$. Here, $v_p = v_p(z,t)$ denotes the dimensionless in-flow velocity of the melt in normal direction at the melt front. Furthermore, $Q_A = Q_A(z,t)$ and the constant Q_s are dimensionless heat flow densities at the absorption front and in the solid phase at the melt front, respectively. Here, Q_A is a function of the Fresnel absorption $\mathcal{A} = \mathcal{A}(\mu)$ and the cosine $\mu = \mu(z,t)$ of the angle of incidence of the laser beam onto the absorption front which involves spatial derivatives of h and M. Thus, (1)–(3) yield a nonlinear coupled system of partial differential equations with initial and boundary conditions (4) where m_0 is the distance of the melt front at $z = 0$, and h_i, M_i are initial distributions for h and M at $t = 0$.

Constant positive parameters in this model are the specific heat capacity c_p, the difference ΔT between melting and ambient temperature, the enthalpy of fusion H_m, the beam radius w_0, the mass density ρ, the material absorption parameter ι, the thickness d of the workpiece, the dynamical viscosity η_l and the shear stress τ_g of the cutting gas along the absorption front. Parameters which can be used as optimization variables are the laser power P_L and the cutting velocity v_0. All parameters are given in corresponding physical units.

We use scaled and dimensionless coordinates $x = \tilde{x}/d_m$, $z = \tilde{z}/d$, $t = v_0\tilde{t}/d_m$ and obtain the scalings $h = \tilde{h}/d_m$, $M = \tilde{M}/d_m$ where the $\sim$ superscript indicates that the quantity is given in its corresponding physical unit. The quantity d_m is a typical length for the melt film thickness. The in-flow velocity v_p is scaled by $v_p = \tilde{v}_p/v_0$ whereas the heat flow densities are scaled by $Q = \tilde{Q}/(v_0\rho H_m)$ where, again, $\tilde{v}_p$ and $\tilde{Q}$ are given in corresponding physical units.

To deduce the model, we consider the implicit description

$$\Phi_M(x,z,t) := x_L(t) + M(z,t) - x = 0 \tag{5}$$

for the melt front at $x = x_M$ and the dynamical behavior of a particle (x, z) along this surface which yields

$$\frac{d}{dt}\left(\Phi_M(x(t), z(t), t)\right) = 1 + v_{z,M}\frac{\partial M}{\partial z} + \frac{\partial M}{\partial t} - v_{x,M} = 0 \tag{6}$$

Here, $v_{x,M} = v_{x,M}(z,t)$ and $v_{z,M} = v_{z,M}(z,t)$ denote the dimensionless velocities of the melt front in x– and z–direction, respectively, which can be substituted by means of the dimensionless in-flow velocity v_p of the melt. Denoting $n_M = n_M(z,t)$ as the scaled unit length outer normal vector of the melt along the melt front, we obtain

$$v_p = \langle (v_{x,M}, v_{z,M}), n_M \rangle = \frac{1}{\sqrt{1 + \left(\alpha \frac{\partial M}{\partial z}\right)^2}} \left(v_{x,M} - v_{z,M}\frac{\partial M}{\partial z} \right) \tag{7}$$

at the melt front. Combining (6) with (7) yields

$$\frac{\partial M}{\partial t} = v_p \sqrt{1 + \left(\alpha \frac{\partial M}{\partial z}\right)^2} - 1 = v_p - 1 + O(\alpha^2) \tag{8}$$

For the absorption front $x = x_A$, we consider the transformation $\bar{x} = x_M - x$ and obtain the implicit form

$$\Phi_A(\bar{x}, z, t) := h(z,t) - \bar{x} = 0 \tag{9}$$

which can be used to deduce a kinematic boundary condition from

$$\frac{d}{dt}\left(\Phi_A(\bar{x}(t), z(t), t)\right) = v_{z,A}\frac{\partial h}{\partial z} + \frac{\partial h}{\partial t} - v_{\bar{x},A} = 0 \tag{10}$$

In [7] we obtain that the relative velocities $v_{\bar{x},A}$ and $v_{z,A}$ of the absorption front in $\bar{x}$– and z–direction are given by

$$v_{\bar{x},A} = v_p + O(\alpha), \quad v_{z,A} = 2h + O(\alpha) \tag{11}$$

The expression for d_m can be deduced from [8] which implies $\alpha \ll 1$ in a realistic cutting process. Neglecting therefore terms of order $O(\alpha)$ in (8) and (11) yields the two first-order partial differential equations in (1). The coupling can be deduced by means of the so-called Stefan condition [4] where the in-flow velocity v_p is given by the jump of the heat flow density at the melt front. Due to the thinness of the melt, we assume that, for fixed z, the heat flow density in the liquid phase is constant which leads to the third equation in (1). The expressions for Q_A and Q_s as well as the other formulae in (2), (3) can be found in [8] where, again, higher order terms in α are neglected. We note that the approximation for μ is only good for values around zero, i.e. for nearly vertical absorption fronts, which is the case in a typical cutting process. The x–position m_0 of the two fronts at $z = 0$ is given by the scaled value w_0/d_m of the beam radius. For this model we assume no interaction of the lower boundary at $z = 1$ with the melt. Hence, we consider $z \in [0, \infty)$ in the following theoretical discussions.

3 Linear stability analysis

In this section, we perform a linear stability analysis of the system (1)–(4). We introduce a perturbation parameter $\epsilon > 0$ and investigate (1)–(4) by using the initial condition

$$h_i = h_0 + \epsilon g_h, \quad M_i = M_0 + \epsilon g_M \tag{12}$$

where $h_0 = h_0(z)$ and $M_0 = M_0(z)$ are stationary solutions of (1)–(4) and $g_h = g(z)$, $g_M = g_M(z)$ are initial perturbations in the system, e.g. given by a sinusoidal wave with fixed frequency. We partition the solution by

$$h = h_0 + \epsilon h_1, \quad M = M_0 + \epsilon M_1 \tag{13}$$

where $h_1 = h_1(z,t)$ and $M_1 = M_1(z,t)$ describe the dynamical behavior of the initial perturbations g_h, g_M. We consider the Taylor expansion of the absorption $\mathcal{A}$ around the stationary value μ_0 of μ given by

$$\mathcal{A}(\mu) = \mathcal{A}(\mu_0) + \epsilon\mu_1\mathcal{A}'(\mu_0) + O(\epsilon^2), \quad \mu = \mu_0 + \epsilon\mu_1. \tag{14}$$

where the partition of μ is a direct consequence of (13) and (3).

In the following, we suppose $\mu_0 \geq 0$ since $\mu_0 < 0$ implies that the laser beam hits the absorption front from inside the melt which is, from the physical point of view, not reasonable.

Lemma 1. *A stationary solution of (1)–(4) with $\mu_0 \geq 0$ exists if and only if*

$$0 < r < 2\iota, \quad r = \frac{1+Q_s}{\nu} \tag{15}$$

holds. In this case, the solution is unique and given by

$$h_0(z) = \sqrt{z}, \quad M_0(z) = \sqrt{z} - \frac{1}{\alpha}\mu_0 z + m_0, \quad \mu_0 = \frac{\iota r}{\sqrt{(4\iota - r)r} - r} \tag{16}$$

Proof. We substitute (13) and (14) into (1)–(4) and consider terms of order $O(1)$ in ϵ to obtain two solutions $\mu_0^{(1)}$ and $\mu_0^{(2)}$ given by

$$\mu_0^{(1)} = \frac{\iota r}{\sqrt{(4\iota - r)r} - r}, \quad \mu_0^{(2)} = \frac{\iota r}{-\sqrt{(4\iota - r)r} - r}, \quad r = \frac{1+Q_s}{\nu} \tag{17}$$

for the stationary value μ_0 of μ. Hence, for $r > 4\iota$, i.e. large values of v_0 or small values of P_L, there exists no stationary solution. Furthermore, for all $r \leq 4\iota$, we obtain $\mu_0^{(2)} < 0$ which contradicts the assumption $\mu_0 \geq 0$. Since $r > 2\iota$ implies $\mu_0^{(1)} < 0$ and $r = 2\iota$ provides no solution for $\mu_0^{(1)}$, the only possible setting is $r < 2\iota$ (i.e. small v_0 or large P_L) which leads to the stationary solutions given in (16).

Remark 1. We note that in this model μ_0 and hence the angle of incidence of the laser beam onto the absorption front is constant for all z.

Considering terms of order $O(\epsilon)$ yields the linear perturbation system

$$\frac{\partial y}{\partial t} + F\frac{\partial y}{\partial z} = Ny, \quad y(0,t) = \begin{pmatrix} 0 \\ 0 \end{pmatrix}, \quad y(z,0) = \begin{pmatrix} g_h(z) \\ g_M(z) \end{pmatrix} \tag{18}$$

$$F = F(z) = \begin{pmatrix} 2h_0 - c_0 & c_0 \\ -c_0 & c_0 \end{pmatrix}, \quad N = N(z) = \begin{pmatrix} -1/h_0 & 0 \\ 0 & 0 \end{pmatrix} \tag{19}$$

for the vector perturbation $y = (h_1, A_1)^T$ with, using (16),

$$c_0 = \alpha\nu\left(\mathcal{A}(\mu_0) + \mu_0\mathcal{A}'(\mu_0)\right) = \alpha(1+Q_s)\frac{2\iota(\iota+\mu_0)}{\mu_0(\iota^2+2\iota\mu_0+2\mu_0^2)} > 0 \tag{20}$$

Lemma 2. *For $z > 0$, the system (18), (19) is hyperbolic, elliptic or parabolic if and only if the term $h_0(z) - 2c_0$ is positive, negative or zero, respectively.*

Proof. The eigenvalues of F are given by $h_0 \pm \sqrt{h_0^2 - 2c_0h_0}$. For $z > 0$, i.e. $h_0 > 0$, we obtain two real, two complex or one multiple eigenvalue if the radicant is positive, negative or zero, respectively, which proves Lemma 2.

Remark 2. The system (18), (19) yields an interesting example of a system whose property changes from elliptic via parabolic to hyperbolic while z decreases.

In general, a solution of (18), (19) cannot be given since F and N depend on z. To investigate further properties, we consider for a fixed position $z_0 > 0$, the solution in a small neighborhood $|z-z_0| < \delta$, $z_0-\delta > 0$, where the variation of $h_0(z)$ is small. We denote $c_1 := h_0(z_0)$ and obtain

$$\frac{\partial y}{\partial t} + \bar{F}\frac{\partial y}{\partial z} = \bar{N}y, \quad \bar{F} = \begin{pmatrix} 2c_1 - c_0 & c_0 \\ -c_0 & c_0 \end{pmatrix}, \quad \bar{N} = \begin{pmatrix} -1/c_1 & 0 \\ 0 & 0 \end{pmatrix} \tag{21}$$

with initial condition $y(z,0) = (g_h(z), g_M(z))^T$. Note that we are interested in stability of the system (18), (19), i.e. in particular large variations in h_1, M_1. Thus, it is reasonable to investigate the solutions of (21) which will give, for small times $t \geq 0$, local approximations of the solutions of (18), (19). For a rigorous investigation of error bounds between the solutions of both systems, we refer to [1].

Proposition 1. *The system (21) is linearly unstable.*

Proof. Using Fourier transform with respect to z yields the ordinary differential equation

$$\frac{\partial Y}{\partial t} = \bar{R}Y, \ \bar{R} = \bar{N} - ik\bar{F}, \ Y = Y(k,t) = \frac{1}{2\pi}\int_{-\infty}^{\infty} y(w,t)\exp(-ikw)\,dw \tag{22}$$

Stability of (22) and hence, cf. [6], of (21), can be analyzed by means of the real parts of the two complex eigenvalues $\sigma_{1/2} = \sigma^r_{1/2} + i\sigma^i_{1/2}$ of R partitioned in real and imaginary parts given by

$$\sigma^r_{1/2} = -\frac{1}{2c_1} \pm \sqrt{\frac{\xi + \sqrt{\xi^2+\zeta^2}}{2}}, \quad \sigma^i_{1/2} = -kc_1 \pm \sqrt{\frac{-\xi + \sqrt{\xi^2+\zeta^2}}{2}} \tag{23}$$

$$\xi = k^2 c_1(2c_0 - c_1) + \frac{1}{4c_1^2}, \quad \zeta = k\left(1 - \frac{c_0}{c_1}\right) \tag{24}$$

Since $\zeta = 0$ implies $c_0 = c_1$ and hence $\xi > 0$, we have $\sigma^r_1 > \sigma^r_2$. Therefore, (22) is stable if and only if $\sigma^r_1 \le 0$ holds. Basic calculations yield that this is equivalent to the three conditions

$$\text{(I)}: \ \frac{1}{2c_1} \ge 0, \quad \text{(II)}: \ \frac{1}{2c_1^2} - \xi \ge 0, \quad \text{(III)}: \ -c_0^2 \ge 0 \tag{25}$$

Condition (I) is fulfilled for all $z > 0$. In view of Lemma 2, Condition (II) is satisfied if and only if the system is not elliptic. However, condition (III) is not fulfilled since from (20) we obtain $c_0 \neq 0$. This implies $\sigma^r_1 > 0$ and hence instability of the system.

As shown in Proposition 1, system (21) is unstable since $c_0 \neq 0$. However, the proof illustrates that $c_0 = 0$ implies $\sigma^r_1 = 0$ and hence marginal stability. Therefore, the value of c_0 can be interpreted as a measurement for instability and for decreasing values $c_0 \to 0$ the process becomes more stable. From (20) we conclude that $c_0 \to 0$ holds for $\mu_0 \to \infty$ which, due to (15), is obtained for $r \to 2\iota$. In the limit case $r = 2\iota$, we obtain a marginal stability curve

$$\mathcal{N} = \{(v_0, P_L) \in \mathbb{R}^2 : P_L = C\, v_0\}, \quad C = \frac{(1+Q_s)\pi w_0^2 \rho H_m}{2\iota} \tag{26}$$

which, as mentioned above, cannot be achieved in practice since μ_0 is not defined in this case. Figure 3 shows the nonlinear dependency of c_0 on p

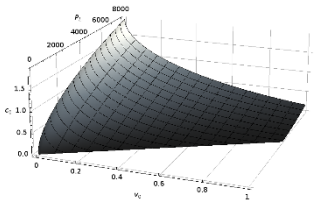

Fig. 3. c_0 as a function of the process parameters v_0 and P_L

where the plot is cut at the curve $\mathcal{N}$ for realistic parameters for stainless steel

$$c_p = 550, \quad \Delta T = 1500, \quad H_m = 277 \cdot 10^3, \quad w_0 = 300 \cdot 10^{-6} \tag{27}$$

$$\rho = 7000, \quad \iota = 0.25, \quad d = 4 \cdot 10^{-3}, \quad \eta_l = 2 \cdot 10^{-3}, \quad \tau_g = 500 \tag{28}$$

It can be deduced that c_0 is strictly monotonuously increasing with P_L and decreasing with v_0 which implies that large values of v_0 and small values of P_L may provide a stationary solution with only small instabilities.

4 Minimizing the roughness of the surfaces

To extend our results about the connection between the process parameters v_0, P_L and stability of the system, we will investigate a nonlinear optimization problem. The goal is to find a process parameter vector

$$p = (v_0, P_L)^T \in P, \quad P \subset P_{\text{ad}} := \{p \in \mathbb{R}^2 : P_L > C\, v_0 > 0\} \tag{29}$$

with C from (26) such that the melt surfaces stay close to the stationary solution. Here, P is an arbitrary non-empty compact and convex subset of P_{ad} where the condition $P_L > C\, v_0$ (which is equivalent to $r < 2\iota$, cf. (15)) in the definition of P_{ad} ensures the existence of a stationary solution due to Lemma 1 and $v_0 > 0$ (note that $C > 0$) is a physically reasonable bound. The problem is to find $p \in P$ which minimizes the roughness

$$\mathcal{R}(p) := \frac{1}{2} \int_0^1 \int_0^{t_f} \Big[(h(z,t;p) - h_0(z;p))^2 + \lambda (M(z,t;p) - M_0(z;p))^2 \Big]\, dt\, dz \tag{30}$$

where $h(z,t;p)$, $M(z,t;p)$ are solutions of (1)–(4) with inital condition (12) using $h_0(z;p)$, $M_0(z;p)$ from (16) as stationary solutions, λ is a weighting parameter and t_f is a suitable chosen final time. We will assume that h_0, h, M_0, M are unique solutions sufficiently smooth with respect to p. Note that for all p the system is not stable. Hence, a solution of the optimization problem will yield parameters where the surface roughness is as small as possible.

We present a numerical solution of problem (30). The spatial and time domain is partitioned into $N_z = 80$ and $N_t = 1600$ intervals of length h_z and h_t, respectively. We use the Lax-Wendroff [5] and an Euler-forward scheme for the equation for h and M, respectively. The derivatives in μ are treated by an upwind method. The cost functional (30) is approximated by the composite trapezoidal rule. Using data (27), (28) yields $C = 4362.164$. We choose

$$\epsilon = 0.025, \quad g_h(z) = \sin(5 \cdot 2\pi z) = 10 g_M(z), \quad t_f = 0.8, \quad \lambda = 10 \tag{31}$$

The domain $P \in P_{\text{ad}}$ is taken as

$$0.01 \le v_0 \le 0.2, \quad 100 \le P_L \le 6000, \quad P_L \ge 1.5\, C\, v_0 \tag{32}$$

Using the code IPOPT [13] together with the modeling language AMPL [2], we obtain two local minima p_1 and p_2 of $R(p)$ in P given by

$$p_1 = (0.019995, 180.80)^T, \quad p_2 = (0.2, 6000)^T \tag{33}$$

with $R(p_1) = 0.2500914087$ and $R(p_2) = 0.4751724227$ where p_1 is close to $\mathcal{N}$ and p_2 is at the boundary of P far away from $\mathcal{N}$. Hence, there exists a domain where the roughness decreases for p approaching $\mathcal{N}$ which is equal to the results in the previous section. However, p_1 is strictly inside P close to the boundary and there exists a second minimum. A possible interpretation for these discrepancies with the linear stability analysis is that there are nonlinear effects in the system which can lead to a surface with small roughness although the process is strongly linear instable. Figure 4 shows the solution for h and M for the parameter p_1.

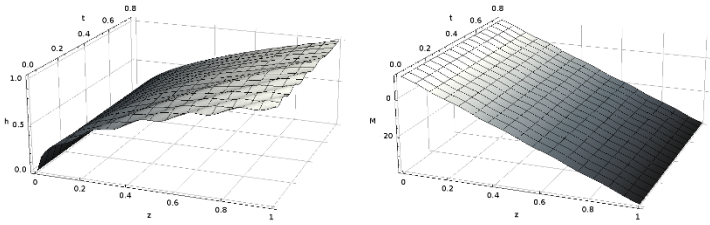

Fig. 4. Melt thickness h (left) and position M of the melt front (right)

We emphasize that p_1 is no realistic parameter vector since P_L is not large enough to melt the workpiece. This can also be seen from the mathematical point of view since μ_0 in this case is so large that at $z = 1$ the absorption front has left the area $[-m_0, m_0]$ of the laser beam, i.e. $M_0(1) < -m_0$. Adjusting P by adding this constraint $\mu_0 \leq \alpha(1 + 2m_0)$, we obtain the only minimum p_2.

5 Conclusions and Outlook

We presented a model for the dynamical behavior of the free melt surfaces in a laser cutting process which involves two nonlinear coupled partial differential equations. We identified parameter domains for the existence of a stationary solution and showed uniqueness in this case. We applied a linear stability analysis to an approximate model and obtained that the system is linearly unstable. This investigation implied that the distance of the parameter vector to a practically not achievable neutral stability curve is a measurement for instability of the system providing rough cutting surfaces. As a second approach, we formulated a nonlinear optimization problem. The goal was to find parameters which minimize the roughness of the cutting surface defined by a tracking cost functional measuring the L_2 distance to the stationary solution. A numerical solution was presented which showed that in a certain domain the results correspond to the linear stability analysis. However, presumedly due to nonlinear effects, we obtained a second local minimum far away from the neutral stability curve. We finally identified a further condition for the technically relevant parameter domain leading to only this second minimum.

Future works comprise extension of the model by non-vertical beam incidence, nonlinear stability analyis (which may lead to explanations for the second minimum), study of necessary and sufficient optimality conditions and the consideration of further, also spatial and time dependent optimization variables which leads to optimal control problems.

6 Acknowledgement

The research related to this paper is supported by the German Research Foundation DFG as part of the Cluster of Excellence "Integrative Production Technology for High-Wage Countries" at RWTH Aachen University.

References

1. Colombo RM, Mercier M, Rosini MD (2009) Stability estimates on general scalar balance laws. C R Acad Sci Paris, Ser I 347
2. Fourer R, Gay DM, Kernighan (1990) A Modeling Language for Mathematical Programming. Management Science 36:519554
3. Friedrich R, Radons G, Ditzinger T, Henning A (2000) Ripple Formation through an Interface Instability from Moving Growth and Erosion Sources. Phys Rev Lett 85:4884-4887
4. Lamé G, Clapeyron BD (1831) Mémoire sur la solidification par refroidissement d'un globe liquide. Ann Chimie Physique, 47:250-256
5. Lax PD, Wendroff B (1960) Systems of conservation laws. Commun Pure Appl Math 13:217-237
6. Kevorkian J (2000) Partial Differential Equations: Analytical Solution Techniques. 2nd Edition. Springer, New York
7. Nießen M (2005) Numerische Modellierung freier Randwertaufgaben und Anwendung auf das Laserschneiden. PhD thesis, RWTH Aachen University
8. Schulz W (2003) Die Dynamik des thermischen Abtrags mit Grenzschichtcharakter. Aachen, Shaker-Verlag, Habilitation thesis, RWTH Aachen University
9. Schulz W, Nießen M, Eppelt U, Kowalick K (2009) Simulation of Laser Cutting. In: Dowden JM (ed) The Theory of Laser Materials Processing: Heat and Mass Transfer in Modern Technology. Springer Series in Materials Science 119
10. Schulz W, Kostrykin V, Nießen M, Michel J, Petring D, Kreutz EW, Poprawe R (1999) Dynamics of Ripple Formation and Melt Flow in Laser Beam Cutting. J Phys D: Appl. Phys. 32:1219-1228
11. Theißen K (2006) Optimale Steuerprozesse unter partiellen Differentialgleichungs-Restriktionen mit linear eingehender Steuerfunktion. PhD thesis, University of Münster
12. Vossen G, Schulz W (2009) Multiple Scale Methods for Nonlinear Stability Analysis in Laser Cutting Processes. Technical Report, RWTH Aachen. Online: http://www.nld.rwth-aachen.de/
13. Wächter A, Biegler LT (2006) On the Implementation of an Interior-Point Filter Line-Search Algorithm for Large-Scale Nonlinear Programming. Mathematical Programming 106(1):25-57